Electronic Supplementary Material (ESI) for Dalton Transactions.

Supporting Information:

Vapor-assisted synthesis of the MOF-74 metal-organic framework family from zinc, cobalt, and magnesium oxides

Nathalie Wauteraerts[a], Min Tu[a,b], Nicolas Chanut[a], Sabina Rodríguez-Hermida[a,c], Jesus Gandara Loe[a] and Rob Ameloot[a*]

[a] Department of Microbial and Molecular Systems, Center for Membrane Separation, Adsorption, Catalysis and Spectroscopy (cMACS), KU Leuven – University of Leuven, Celestijnenlaan 200F, 3001 Leuven, Belgium.

[b] 2020 X-Lab and State Key Laboratory of Transducer Technology, Shanghai Institute of Microsystem and Information Technology, Chinese Academy of Sciences, Shanghai 200050, China.

[c] Servizos de Apoio á Investigación, Universidade da Coruña, Campus Elviña s/n 15071, A Coruña, Spain.

E-mail: rob.ameloot@kuleuven.be

METHODS

Powder X-ray diffraction (PXRD). Powder X-ray diffraction (PXRD) patterns were recorded with a Malvern PANalytical Empyrean diffractometer. A Cu source (Cu Kα1: 1.5406 Å; Cu Kα2: 1.5444 Å) and a PIXcel3D solid-state detector was used. The measurements were performed in transmission mode over 3–45° 2θ range with a step size of 0.0131° and a scan speed of 0.0417 °/s.

In situ XRD measurements of the vapor-assisted synthesis were performed at the P02.1 beamline in the DESY synchrotron (Hamburg, Germany) with a photon energy of 60 keV. The diffractograms were recorded using a Perkin Elmer XRD1621 detector. Also, additional diffraction measurements were performed at the 5.2L SAXS beamline at the Elettra synchrotron (Trieste, Italy) with a photon energy of 8 keV. The diffractograms were recorded using a Pilatus3 1M detector. One third of the 1.0 mm diameter capillary was first filled with metal oxide powder, then a thinner 0.7 mm diameter capillary was filled with liquid additive and placed inside of the thicker capillary, which was subsequently sealed by a butane torch.

The extent of reaction (α) for the different phases was determined by the integration of the peak of the strongest reflection of each phase. First, all diffractograms were corrected for the baseline. Subsequently, the peaks of the strongest reflection of each phase was integrated. At last, the integrated intensities were normalized for each phase separately.

Simulated powder patterns were obtained from the CCDC database and visualization of the crystal structures was done using Mercury.

Thermogravimetry. Thermogravimetric analysis was performed using a Netzsch STA 449 F3 Jupiter thermogravimetric analyzer. A heating rate of 1 °C min^{-1} and a temperature range of 25-800 °C was applied. The measurements were performed under N_2 and air atmosphere.

SEM. SEM measurements were recorded using a Philips XL30 FEG using secondary electrons at 15 kV and a working distance of 10 mm.

N_2 and CO_2 adsorption. N_2 and CO_2 adsorption isotherms were recorded using a Micromeritics 3Flex adsorption analyzer. The N_2 adsorption measurements were performed at 77K. For CO_2 adsorption measurements, the external cooling bath is kept at 25 °C. Prior to the measurements, the samples were extracted with methanol using a Soxhlet extractor for 24 h. Subsequently, the samples were activated under dynamic vacuum at 150 °C for 12 h.

FTIR spectroscopy. Infrared spectra were recorded in the range of 700-4000 cm^{-1} (64 scans/spectrum) with a Varian 670 FTIR spectrometer equipped with an MCT detector.

SUPPLEMENTARY FIGURES

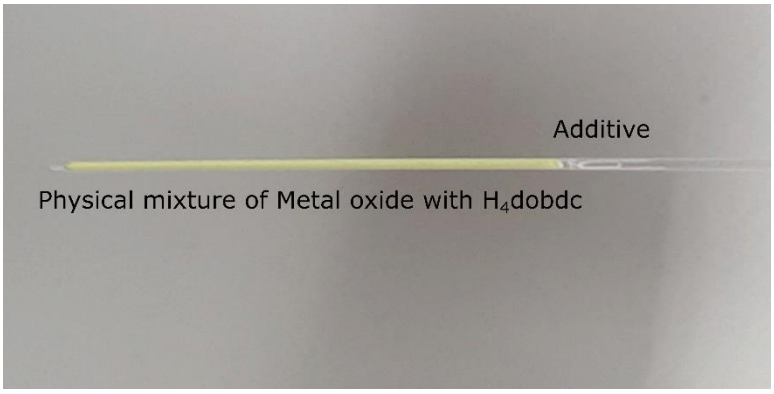

Figure S1: Picture of the capillary setup. The physical mixture is inserted into a 1.5 mm diameter capillary. Afterwards, a smaller capillary (diameter 0.7 mm) containing a small amount of additive is inserted, and the outer capillary is sealed.

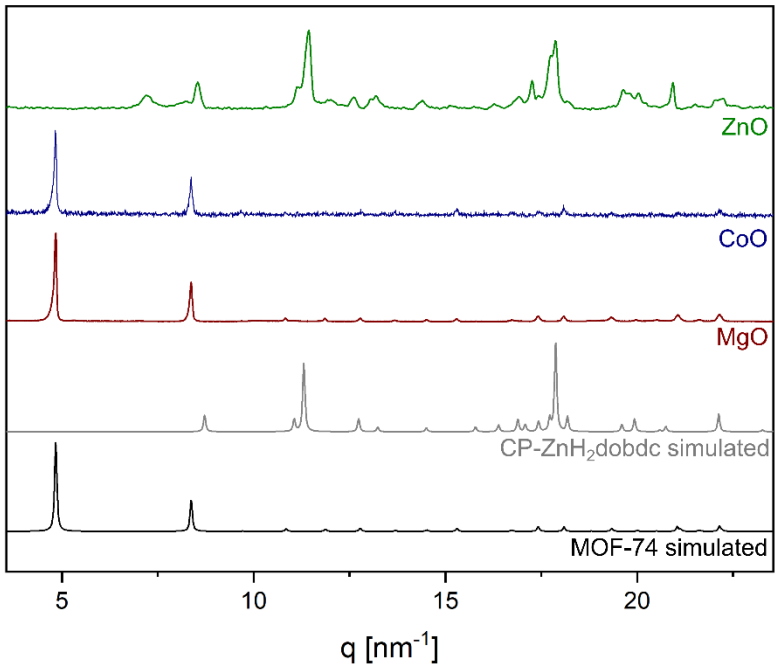

Figure S2: X-ray diffractograms of the reaction products of metal oxides (MgO, ZnO and CoO) with H_4dobdc in the presence of H_2O vapor at 100 °C with a conversion time of 24 h. MgO and CoO are converted to MOF-74. ZnO is converted to a dense coordination polymer, $[Zn(H_2O)_2(H_2dobdc)]_n$ (CCDC: ODIPOH01).

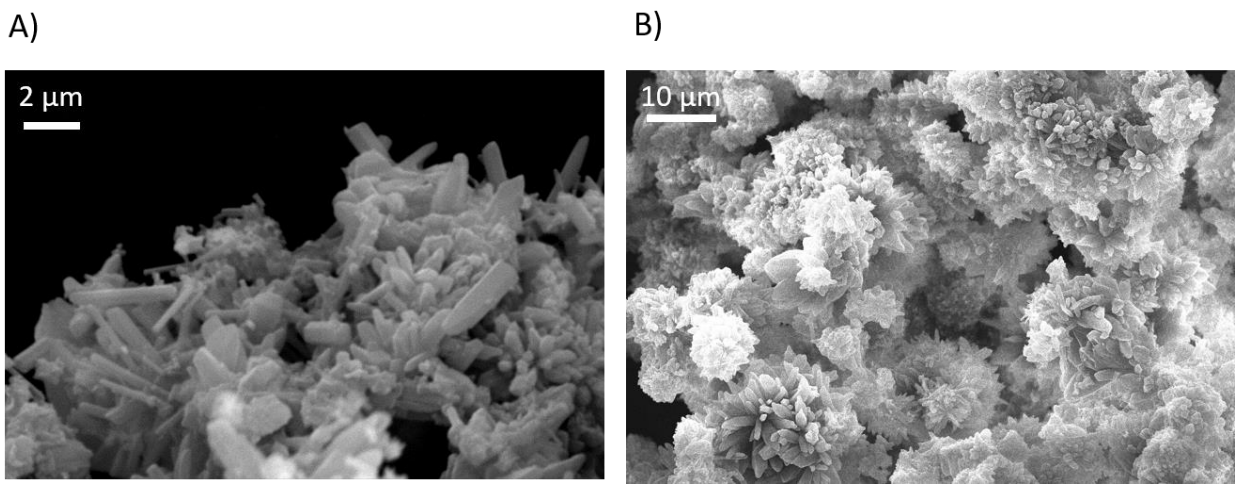

Figure S3: SEM images of MOF-74 with Co (a) and Mg (b) metal nodes, synthesized by the vapor-assisted method in the presence of H_2O vapor.

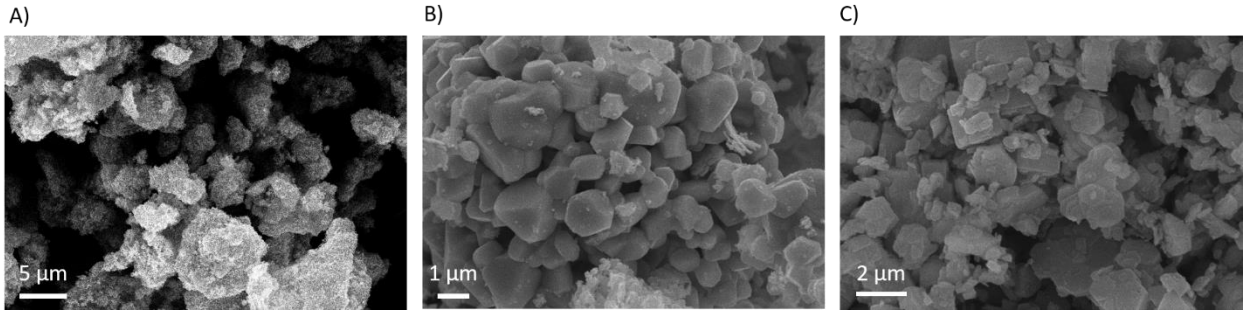

Figure S4: SEM images of metal oxide precursors ZnO (a), CoO (b) and MgO (c).

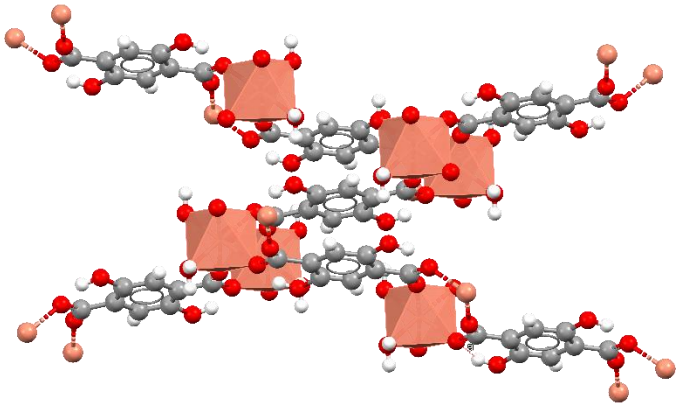

Figure S5: Crystal structure of CPO-26, $Mg(H_2dobdc)(H_2O)_2$ (CCDC: VOGTER).

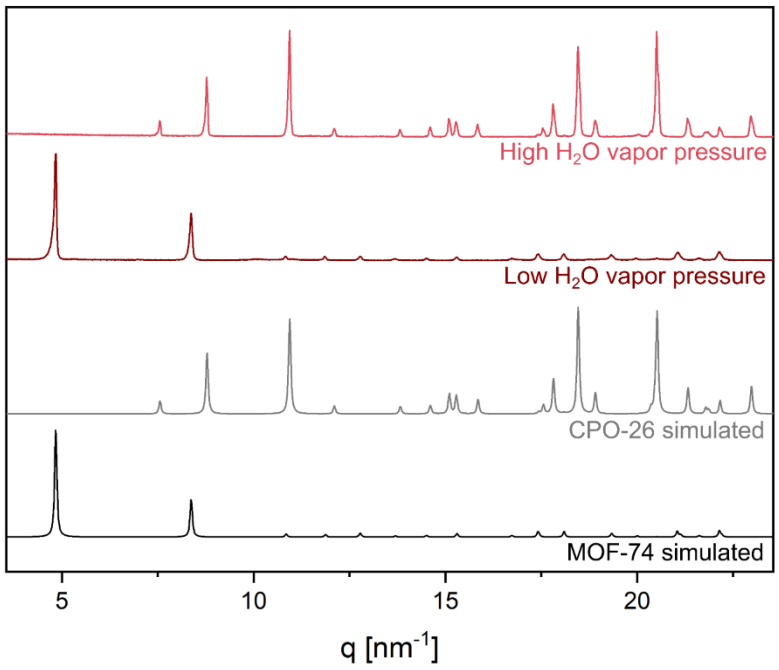

Figure S6: X-ray diffractograms of the vapor-assisted synthesis of Mg-MOF-74 in humid atmosphere at 130 °C with a conversion time of 24 h. When the vapor pressure of H_2O is below the saturation pressure, MOF-74 is obtained. In contrast, a non-porous structure, CPO-26, is obtained when the vapor pressure of H_2O is increased above the saturation pressure.

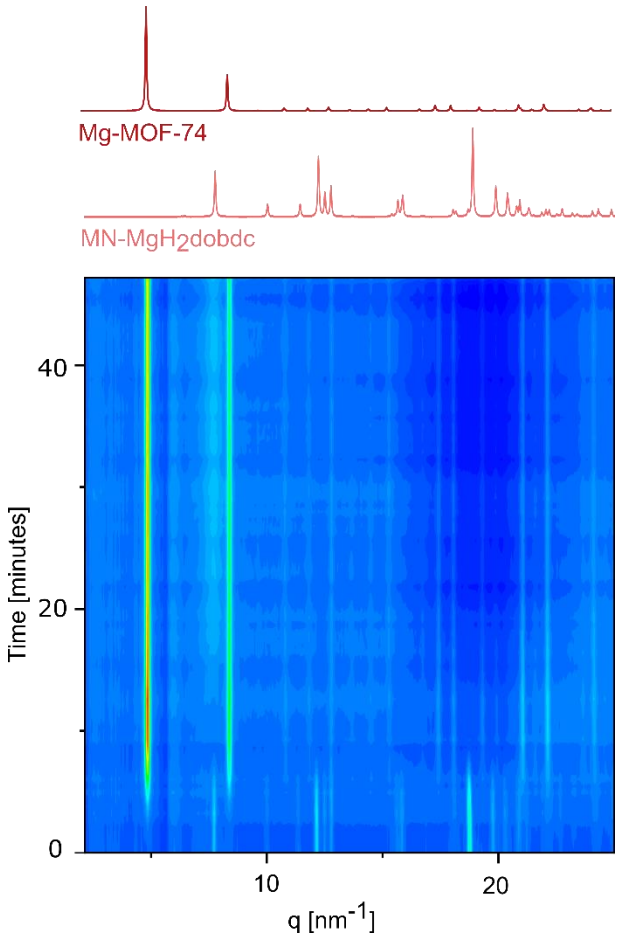

Figure S7: *In situ* X-ray diffraction measurements of the vapor-assisted synthesis of Mg-MOF-74 in a humid atmosphere at 130 °C measured at the P02.1 beamline DESY synchrotron.

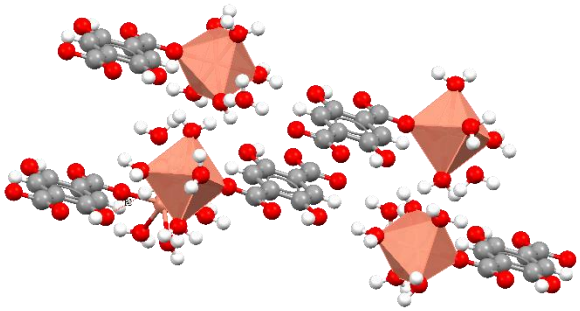

Figure S8: Crystal structure of MN-MgH_2dobdc, Mg(H_2dobdc)(H_2O)$_5$.H_2O (CCDC: XAJGEX).

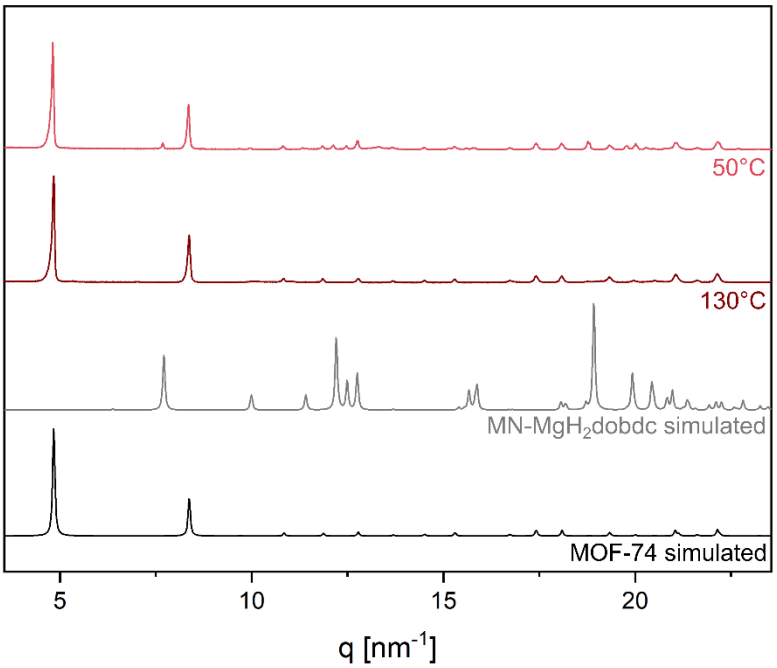

Figure S9: X-ray diffractograms of the vapor-assisted synthesis of Mg-MOF-74 in humid atmosphere at 50 °C and 130 °C with a conversion time of 24 h. At 130 °C, Mg-MOF-74 is formed. At lower temperature (50 °C) an additional phase, Mg(H_2dobdc)(H_2O)$_5$.H_2O (here denoted as MN-MgH_2dobdc) can be observed.

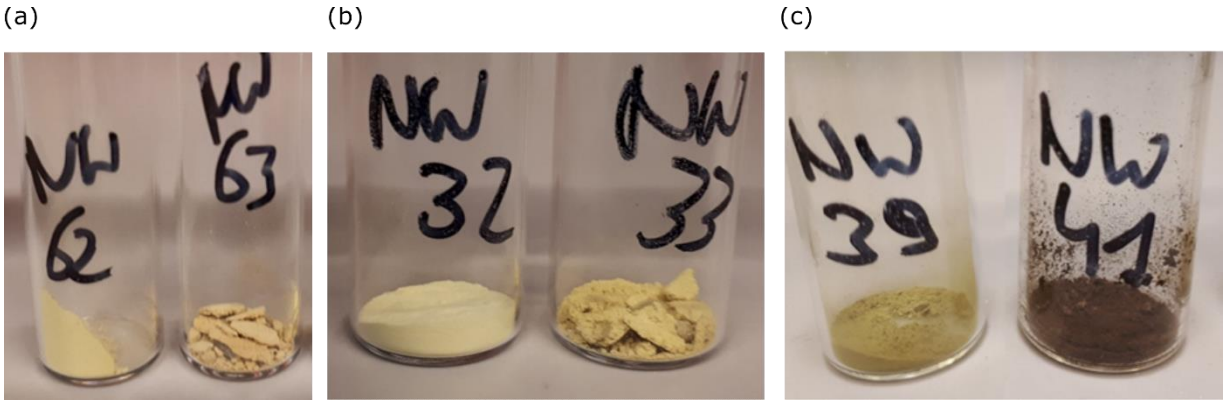

Figure S10: Reaction products of MgO (a), ZnO (b) and CoO (c) with H_4dobdc at 130 °C without (left) and with (right) H_2O vapor.

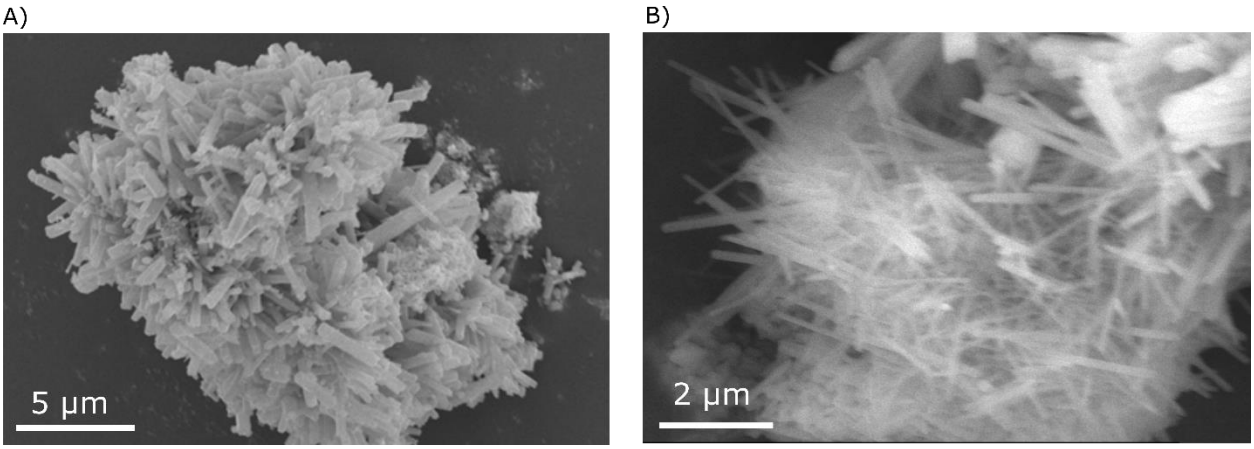

Figure S11: SEM image of Zn-MOF-74 (a) and Zn-UTSA-74 (b) synthesized by vapor-assisted method.

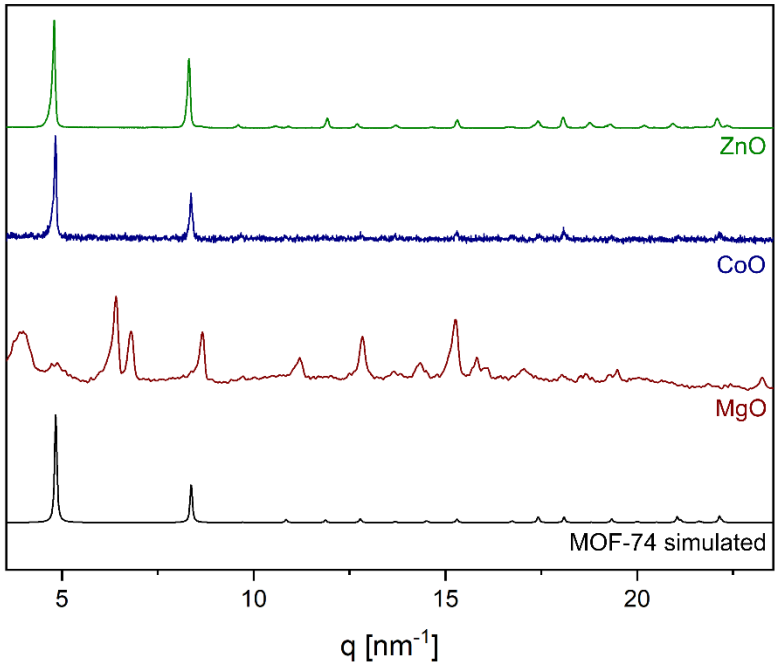

Figure S12: X-ray diffractograms of the reaction products of metal oxides (MgO, ZnO and CoO) with H_4dobdc in the presence of DMF vapor at 100 °C with a conversion time of 24 h. ZnO and CoO are converted to MOF-74. For MgO, an unknown phase can be observed.

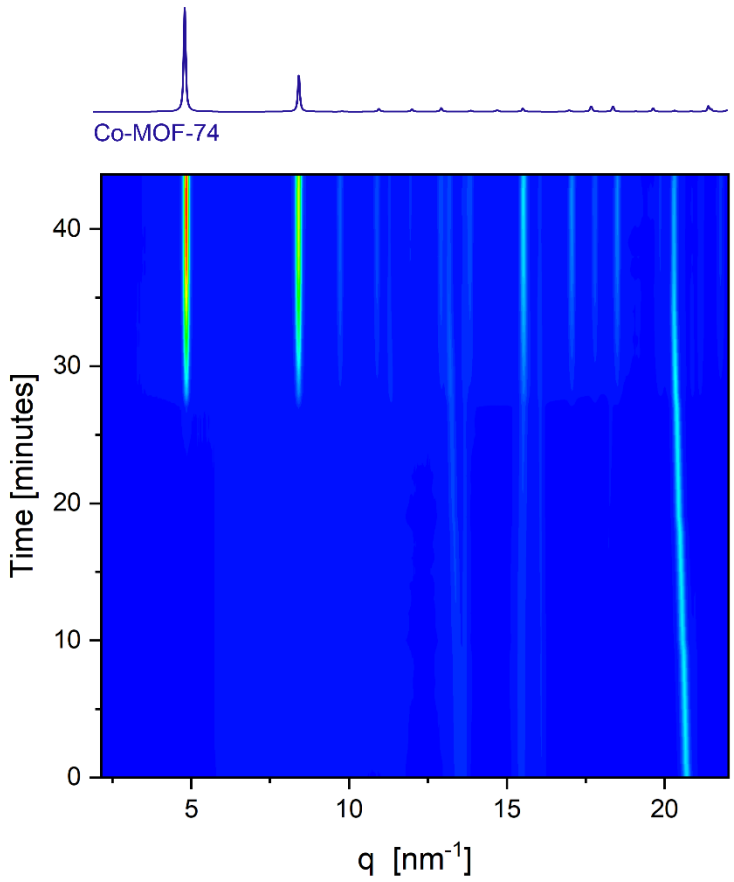

Figure S13: *In situ* X-ray diffraction measurements of the vapor-assisted synthesis of Co-MOF-74 with DMF as additive at 150 °C at the P02.1 beamline DESY synchrotron. The peaks appearing at the start of the measurement originate from diffraction of the linker, H_4dobdc.

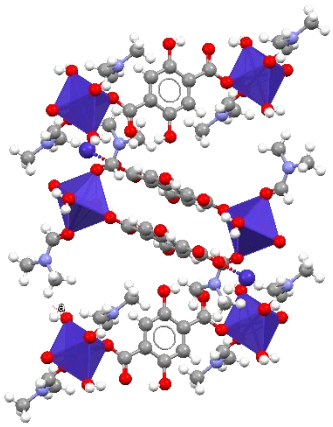

Figure S14: Crystal structure of $Co(dobdc)(DMF)_2(H_2O)_2$ (CCDC: SEWXIE).

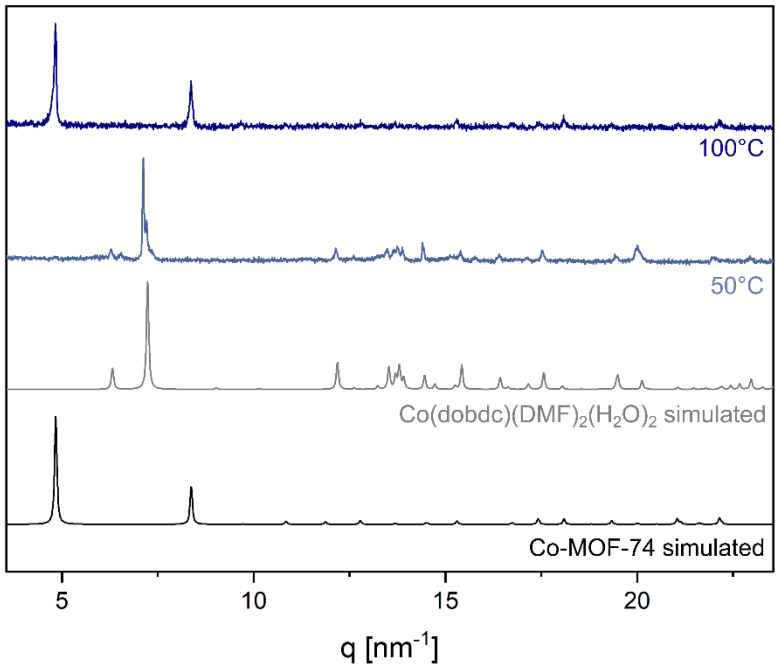

Figure S15: X-ray diffractograms of the vapor-assisted synthesis of Co-MOF-74 with DMF as additive at 50 °C and 130 °C with a conversion time of 24 h. At 100 °C, Co-MOF-74 is formed. At lower temperature (50 °C) $Co(dobdc)(DMF)_2(H_2O)_2$ can be observed.

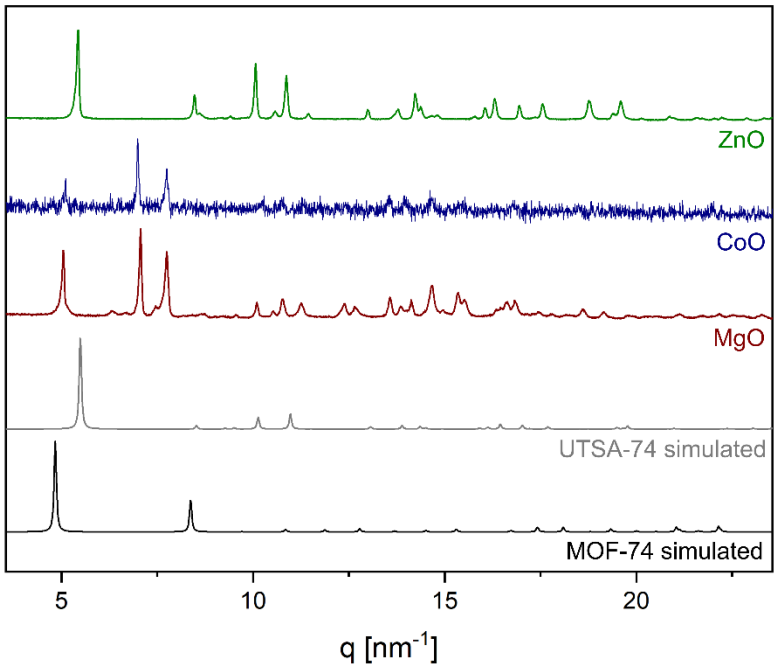

Figure S16: X-ray diffractograms of the reaction products of metal oxides (MgO, ZnO and CoO) with H_4dobdc in the presence of DMSO vapor at 130 °C with a conversion time of 24 h. ZnO is converted to UTSA-74. For MgO and CoO, an unknown phase can be observed.

Table S1: Conversion of metal oxide into M_2dobdc based on TGA measurements (**Figure 3**). The decomposition stage (200 °C-500 °C) is divided in two steps: decomposition of the framework and the degradation of the organic linker.[1,2] The theoretical weight loss for full metal oxide conversion is calculated based on the fact that the decomposition of the MOF structure at high temperature in the presence of oxygen yields metal oxide (Co_3O_4 in case of Co-MOF-74, confirmed by XRD). To calculate the experimental weight loss percentage, the first step in the TG curve resulting from removal of solvents (<200 °C) is not taken into account and only the second step resulting from decomposition of the samples (>200 °C) is considered.

	Theoretical weight loss [%]	Experimental weight loss [%]
Mg_2(dobdc)	66.8	61.8
Zn_2(dobdc)	49.9	52.7
Co_2(dobdc)	48.5	43.2

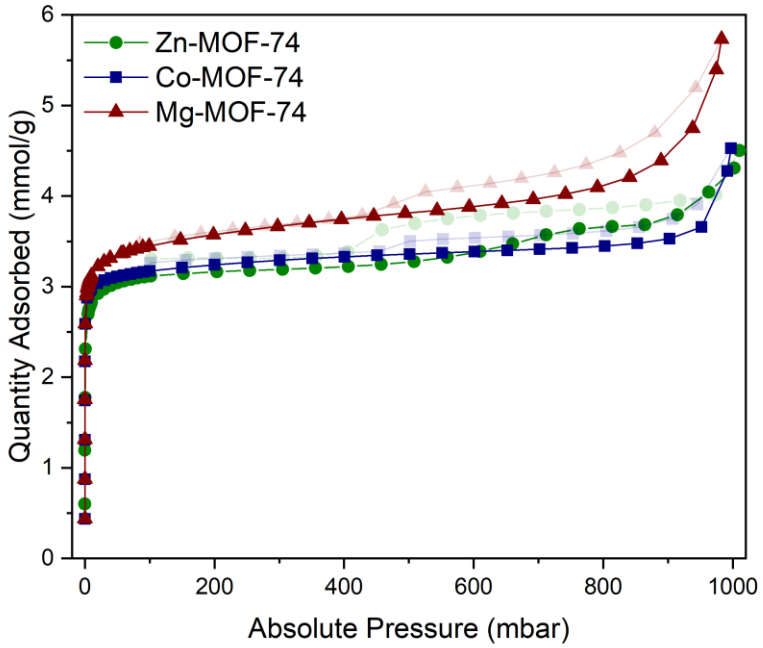

Figure S17: N_2 adsorption isotherms of M-MOF-74 (M = Mg, Co and Zn) after activation at 150°C.

Table S3: Overview of BET surface area of M_2dobdc (M = Mg, Zn and Co) reported in literature.

	BET surface area [m^2/g]	Reference
Mg_2(dobdc)	1525	[4]
	1800	[6]
	1630	[7]
	1495	[12]
Zn_2(dobdc)	1134	[13]
	816	[14]
Co_2(dobdc)	928	[3]
	1404	[9]
	1358	[10]
	1314	[11]
	1356	[13]
	1080	[12]

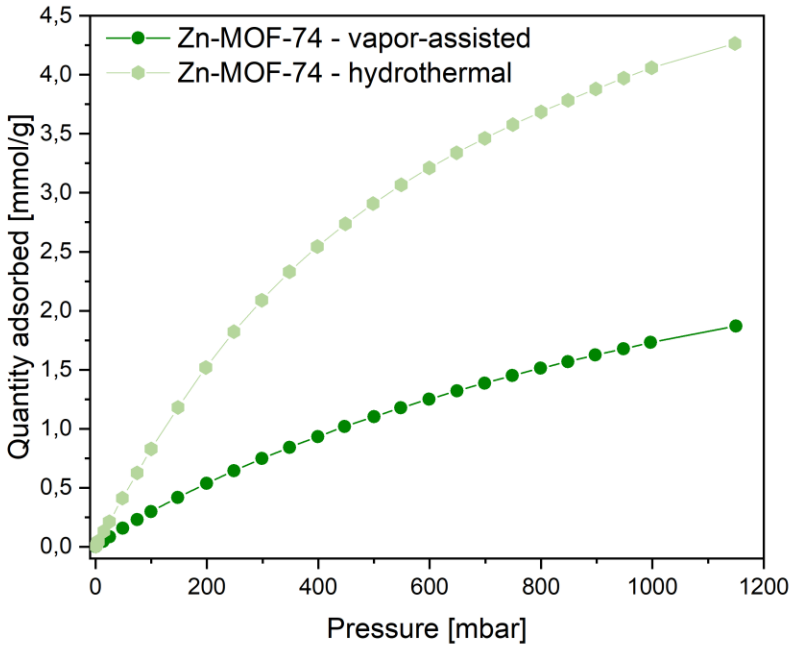

Figure S18: CO_2 adsorption isotherms of Zn-MOF-74 synthesized via vapor-assisted approach and via hydrothermal approach, recorded at 25°C.

Table S2: Overview of CO_2 capacity of M_2dobdc (M = Mg, Zn and Co) reported in literature.

	CO_2 capacity at 298K [mmol/g]	Reference
Mg_2(dobdc)	9	[3]
	7.9	[4]
	1.2	[5]
	±9	[6]
	8	[7]
Zn_2(dobdc)	5.9	[3]
	1.6	[5]
Co_2(dobdc)	6.9	[3]
	6.6	[8]
	3.67	[9]
	6.65	[10]
	6.5	[11]

The PXRD diffractograms of the Zn-MOF-74 samples synthesized via the vapor-assisted and hydrothermal approaches were quantitatively analyzed to determine their amorphous content. To this end, we applied the Reference Intensity Ratio (RIR) method, which is based on the principle that the peak intensity of a crystalline phase is correlated to its concentration in a mixture. For this analysis, we used Si powder as the reference material that is assumed to be fully crystalline. First, different mixtures of the hydrothermally synthesized Zn-MOF-74 and Si were made with known mass ratios to construct a calibration curve. For our analysis, the peak intensities of the strongest reflections of each phase were taken into account, namely [2 -1 0] for Zn-MOF-74 and [1 1 1] for Si. Subsequently, the fraction of MOF-74 phase in the vapor-assisted synthesized sample can be estimated using the calibration curve.

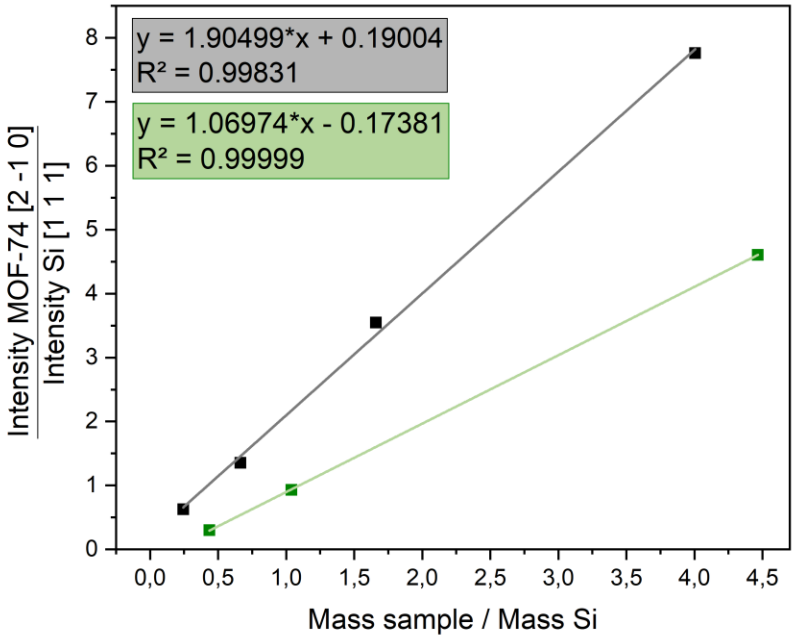

Figure S19: RIR method based on PXRD of the hydrothermal synthesized Zn-MOF-74 sample. The peak intensities of the strongest reflection is used which is [2 -1 0] for Zn-MOF-74 and [1 1 1] for Si. The green square indicates the values obtained for the vapor-assisted method.

Characteristic peaks that differentiate coordinated and (partially) uncoordinated linkers are the carbonyl (1650 cm^{-1}), C-OH (1200 cm^{-1}), and hydroxyl stretching (3100 cm^{-1}) modes. These peaks are replaced by asymmetrical (1550 cm^{-1}) and symmetrical stretching (1410 cm^{-1}) of carboxylate groups in the MOF material (**Figure S18**).[16] The FTIR spectra of samples obtained through the vapor-assisted approach and the hydrothermal reference method were compared. For both synthesis methods, a broad peak at 3352 cm^{-1} indicates adsorbed water. The spectra of the Mg and Co-variant synthesized by the vapor-assisted method match the hydrothermally synthesized sample of the Zn-form. In contrast, the spectrum of Zn-MOF-74 obtained through the vapor-assisted approach shows two additional peaks: at 1650 cm^{-1} and 1289 cm^{-1}. Both peaks can also be observed in the spectrum of the uncoordinated, protonated linker molecule. Note that only the carbonyl peak at 1650 cm^{-1} can be observed since the other characteristic peaks for the linker molecule at 3100 cm^{-1} and 1200 cm^{-1} overlap with other peaks in the MOF-74 spectrum. This result indicates that not all linker molecules are fully coordinated in the Zn-MOF-74 sample obtained through vapor-assisted conversion. In the Co-MOF-74 and Mg-MOF-74 samples prepared in the same way, the carboxylate groups of the linker are fully coordinated.

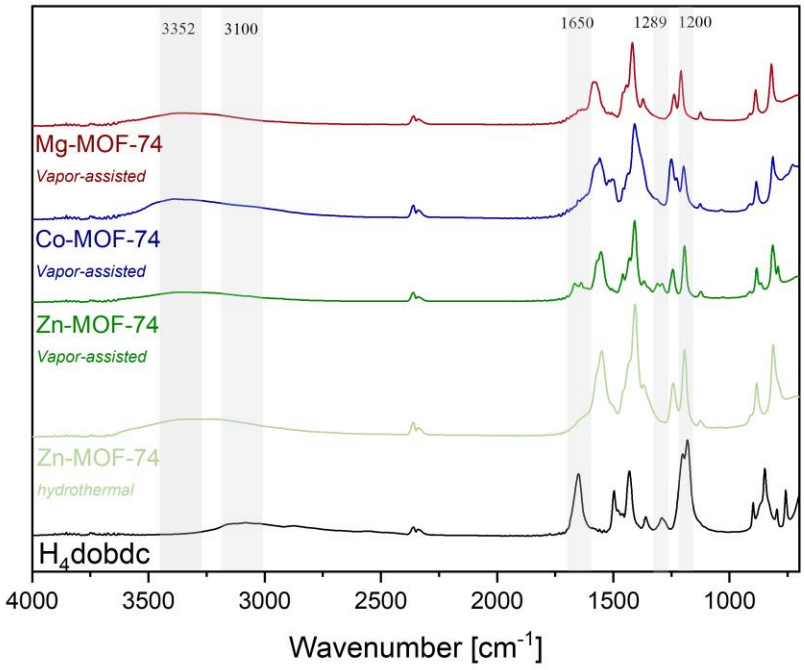

Figure S20: FTIR measurements of M-MOF-74 (M = Mg, Zn and Co). Comparison between vapor-assisted synthesis method and hydrothermal approach for Zn-MOF-74.

REFERENCES

1 G. Ayoub, B. Karadeniz, A. J. Howarth, O. K. Farha, I. Đilović, L. S. Germann, R. E. Dinnebier, K. Užarević and T. Friščić, *Chem. Mater.*, 2019, **31**, 5494–5501.

2 P. A. Julien, K. Užarević, A. D. Katsenis, S. A. J. Kimber, T. Wang, O. K. Farha, Y. Zhang, J. Casaban, L. S. Germann, M. Etter, R. E. Dinnebier, S. L. James, I. Halasz and T. Friščić, In Situ Monitoring and Mechanism of the Mechanochemical Formation of a Microporous MOF-74 Framework, https://pubs.acs.org/doi/pdf/10.1021/jacs.5b13038, (accessed April 18, 2020).

3 W. L. Queen, M. R. Hudson, E. D. Bloch, J. A. Mason, M. I. Gonzalez, J. S. Lee, D. Gygi, J. D. Howe, K. Lee, T. A. Darwish, M. James, V. K. Peterson, S. J. Teat, B. Smit, J. B. Neaton, J. R. Long and C. M. Brown, *Chem. Sci.*, 2014, **5**, 4569–4581.

4 D.-A. Yang, H.-Y. Cho, J. Kim, S.-T. Yang and W.-S. Ahn, *Energy Environ. Sci.*, 2012, **5**, 6465–6473.

5 Z. Gao, L. Liang, X. Zhang, P. Xu and J. Sun, *ACS Appl. Mater. Interfaces*, 2021, **13**, 61334–61345.

6 J. A. Mason, K. Sumida, Z. R. Herm, R. Krishna and J. R. Long, *Energy Environ. Sci.*, 2011, **4**, 3030–3040.

7 A. A. Godoy, D. Villarroel-Rocha, J. J. Arroyo-Gómez, C. Bernini, G. Narda and K. Sapag, *Materials*, 2023, **16**, 117.

8 J. Hu, L. Li, H. Li, Y. Zhai, F. Tang, Z. Zhang and B. Chen, *RSC Adv.*, 2022, **12**, 33716–33724.

9 A. K. Adhikari and K.-S. Lin, *Chem. Eng. J.*, 2016, **284**, 1348–1360.

10 M. Zhao, Y. Ban, Z. Chang, Y. Zhou, K. Yang, Y. Wang, N. Cao and W. Yang, *AIChE J.*, 2022, **68**, e17528.

11 H.-Y. Cho, D.-A. Yang, J. Kim, S.-Y. Jeong and W.-S. Ahn, *Catal. Today*, 2012, **185**, 35–40.

12 S. R. Caskey, A. G. Wong-Foy and A. J. Matzger, *J. Am. Chem. Soc.*, 2008, **130**, 10870–10871.

13 I. Choi, Y. E. Jung, S. J. Yoo, J. Y. Kim, H.-J. Kim, C. Y. Lee and J. H. Jang, *J. Electrochem. Sci. Technol.*, 2017, **8**, 61–68.

14 A. R. Millward and O. M. Yaghi, *J. Am. Chem. Soc.*, 2005, **127**, 17998–17999.

15 D. Cattaneo, S. J. Warrender, M. J. Duncan, R. Castledine, N. Parkinson, I. Haley and R. E. Morris, *Dalton Trans.*, 2015, **45**, 618–629.

16 K. Tan, S. Zuluaga, Q. Gong, P. Canepa, H. Wang, J. Li, Y. J. Chabal and T. Thonhauser, *Chem. Mater.*, 2014, **26**, 6886–6895.